Green synthesis of Halloysite-Silver Nanocomposite: using Acalypha australisExtract, anti-E. coli effect and gene expression

Zainab Zamel Khalaf

zainab.alnaji@sc.uobaghdad.edu.iq

University of Baghdad

Duaa M.Abdulsatar

Al-Iraqia University https://orcid.org/0000-0002-5536-0463

Heba Khaleel Tawfeeq

University of Baghdad

Nagham Shakir Alattar

University of Baghdad

Research Article

Keywords: Biofilm, E. coli, halloysite nanocomposite, AgNPs, fimH, mrkD

Posted Date: August 10th, 2026

DOI: https://doi.org/10.21203/rs.3.rs-10619350/v1

Additional Declarations: The authors declare no competing interests.

Green synthesis of Halloysite-Silver Nanocomposite: using *Acalypha australis* Extract, anti-E. coli effect and gene expression

Heba Kh. Tawfeeq[1], Nagham Sh. Alattar[1], Duaa M. Abdulsatar[2] and Zainab Zamel Khalaf[1]

[1]*Department of Biology, College of Science, University of Baghdad, Baghdad, Iraq.*
[2] *Microbiology Department, College of Medicine, Al-Iraqia University, Baghdad, Iraq*
*E-mail: zainab.alnaji@sc.uobaghdad.edu.iq

Abstract

Bacterial resistance is a major crisis in the area, leading to increased rates of morbidity and mortality in humans. The use of nanomaterials as a procedure to replace/co-use traditional treatments is a trend in microbiology. In this study, *Acalypha australis* extract was selected for the green-ultrasound assisted synthesize of Ag-Halloysite (NSH) nanocomposite. NSH was characterized by using XRD and TEM while the extract was characterized for its component using GC-Ms. The results demonstrated the presence of halloysite nanorod that decorated with silver nanoparticles. NSH was investigated for its effectiveness in reducing gene expression for *fimH* and *mrkD* genes of pathogenic *E. coli*. *A.* The results demonstrate that NSH markedly reduced the gene expression of *fimH* and *mrkD*. In conclusion, NSH played a crucial role in inhibiting the biofilm of *E. coli* via a potential fimbrial formation inhibition-dependent mechanism.

Keywords: Biofilm, *E. coli*, halloysite nanocomposite, AgNPs, *fimH*, *mrkD*

1. Introduction

Antibiotic resistance might be the utmost concern of the last few decades, making the microorganism thrive and raising the prevalence of bacterial infection as opposed to the rate of healing imposing an ultimate burden on the global medical care network [1-3]. Numerous factors are implicated with antimicrobial resistance among which ecological [4], behavioural [5], and molecular [6] are the most important.

Among the tactics used by bacterial species to increase resistance to the microbicidal compounds is their assemblage in close proximity establishing a matrix that incorporates carbohydrates, proteins, lipids, and nucleic acids, as the overall community referred to as biofilm [7]. The development of biofilm trajectories is species-specific as well as

environmental-dependent on conditions, suggesting that biofilm formation can occur through different mechanisms [8].

Escherichia coli as a commensal microorganism of the human and animal intestine is highly implicated in numerous intestinal and extra-intestinal infections as an opportunistic pathogen [9]. Locally this pathogen is accountable for more than 60% of urinary tract infections [10]. Type 1 fimbriae are involved in bacterial pathogenicity and biofilm establishment, which are vital virulence elements in uropathogenic *E. coli* [11]. The FimH protein serves as the receptor spotting type 1 fimbriae that is placed on the tip of the fimbria and possibly intercalated along the fimbrial shaft [12, 13]. Another important fimbria, type 3 fimbria composed of MrkA, B, C, D, and F proteins which represent, the minor subunit, the chaperone, the usher, the adhesin subunit, and the major subunit, respectively. However, the MrkD adhesin is stationed at the top of this fimbria and controls the adhesion and biofilm formation [14].

Green methods were used to prepare nano silver, as these methods have proven their effectiveness in preparing nano silver, in addition to being a rapid method and can be used to produce significant amounts of nano silver with their effectiveness in generating stable silver for long periods of time, in addition to their biocompatibility due to the lack of use of chemicals in the preparation [15, 16]. These points are what made the green method more effective compared to chemical and physical methods [17]. In the same context, in the preparation methods, ultrasound was used in our work for two purposes, which are to use it as a physical dispersant that increases the amount of SPR and thus achieve high stability, in addition to materials for the interaction between the extract and silver ions, which allows the reaction to be carried out within a very short time frame [18]. Ultrasound was used in the preparation of many nano materials, including nano silver [19] and ferrites [20], in addition to the formation of metal oxides and their clay complexes such as the palladium complex with graphene oxide [18] and the manganese oxide complex with attapulgite [21]. All of these previous studies have proven the effectiveness of this method and its positivity on many environmental and economic levels. Based on the fact that nanomaterials are widely used in biological applications, research continues in an impressive manner to find new materials for the purpose of preventing bacterial growth. On this basis, nanosilver has been widely used for this purpose because it does not show toxicity to living cells [15], which makes it a completely updated platform on a daily basis in the world by researchers. In order to improve its properties, it is supported in nanocomposites to stick it in different applications. Among these composites are the composites of silver with clays [22], where a composite of silver with attapulgite was prepared,

which proved the silver coating of attapulgite channels with the separation of attapulgite bundles and their transformation into nanochannels with a size not exceeding 50 nanometers [22]. This composite was used as an antibacterial in water-based emulsion and proved its high effectiveness. For this reason, in this work, halloysite clay was chosen, which is very similar to attapulgite in structure and morphology, in addition to its low price and biocompatibility [22- 24].

The present study adopted a biogenic approach to synthesize a halloysite-silver nanocomposite (NSH) employing *A. australis* aqueous extract as a reducing agent to test the potential efficacy of NSH on the expression of *fimH* and *mrkD* in *E. coli*.

2. Materials and Methods

2.1 Preparation of Acalypha australis Extract

The leaves of *A. australis* were collected and washed with tap water and then washed with distilled water several times to get rid of impurities and dust. The leaves were then ground, and the powder was expressed through a 1 mm sieve to be ready for the next steps. Afterwards, 10 g of the prepared powder was loaded into the Soxhlet, water (100 ml) was added to the flask as extraction solvent and heating was carried out by thermal escalation at 100°C for 4 hours from the start of boiling. The solution was filtered through a 0.22 µm filter and evaporated in a water bath until the extract was obtained as a thick liquid.

2.2 Gas chromatography-mass spectroscopy

The chemical composition of the samples was determined using GCMS-QP2010 plus (Shimadzu, Japan) mass spectrometer with a direct capillary column TG–5MS (30 m × 0.25 mm × 0.25 m film thickness). Initially, the column oven was set at 50°C; then, the temperature was increased by 5 °C/min to 230 °C, which was held for 2 min, and then by 30°C/min to 290°C, which was also maintained for 2 min. Next, the temperature of the injector and MS transfer lines was held at 250 and 260°C, respectively. Helium was used as a carrier gas at a constant flow rate of 1 mL/min. The solvent delay was 3 min, and 1 µL of the diluted samples was automatically injected using Autosampler AS1300 coupled with GC in the split mode. EI mass spectra were collected at 70 eV ionization voltages over the range of *m*/*z* 40–1000 in full scan mode. Next, the ion source temperature was set to 200°C. Finally, the components were identified by comparing the components' retention times and mass spectra to those of the WILEY 09 and NIST 11 mass spectral databases [25].

2.3 Synthesis of nanocomposite of silver and halloysite

The synthesis of NSH started with the addition of 150 mg of halloysite to 100 mL of *A. australis* extract to 100 mL under sonication with 100% power of ultrasonic probe for 20 min, then 100 mL of 0.0125M $AgNO_3$ solution was added to the mixture, and sonication proceeded for another 20 min. The final colour of the solution was dark-brown, and the procedure was inspired by Zhang and Majd [26]. The colloidal was centrifuged (5000 × g for 20 min), and the supernatant was discarded, then the filtrate was washed with deionized water and re-centrifuged 3 times. The filtrate was collected and dried at 50ºC. The resultant nanoparticles were characterized by XRD and TEM.

2.4 Anibacterial Activity

The well diffusion method was applied to investigate the efficiency of *A. australis* extract and NSH against *E. coli* isolates. Mueller-Hinton agar plates were seeded with 1.5×10^8 CFU/mL of the bacterial suspension. Later, 6 mm wells were cut and 50 µL of *A. australis* extract or NSH were added to each well and the plates were incubated at 37°C for 24 h. Ultimately, the diameters of inhibitory zones were measured in millimetres with the aid of a metric ruler [27].

2.5 Determination of bacterial minimum inhibitory concentration

Three concentrations of 25, 50, and 100% of the *A. australis* extract and NSH were prepared and placed in a 96-well microtiter plate. Simultaneously, bacterial suspension compatible with McFarland standard No. 0.5 was prepared to obtain 10^8 CFU/mL. Afterwards, 100 µL of this suspension was introduced into all wells to reach a final volume of 200 µL. Negative and positive controls were prepared as well. Subsequently, the microplates were incubated aerobically at 37°C for 18 hours and the results were evaluated after three replications. The lowest concentration of antimicrobial agent that completely inhibits the visible growth of microorganisms is known as minimal inhibitory concentration (MIC). Nevertheless, 100 µL of the MIC well and three prior wells were cultured separately on Mueller Hinton agar, and after 24 h of incubation.

2.6 Detection of biofilm-forming capacity

Selected *E. coli* isolates were grown for approximately 18 hours at 37°C in 1% glucose-containing tryptic soy broth. Thereafter, the method described by Bras, et al. [28] was followed, in brief: 200 µL of bacterial isolate suspension was adjusted to McFarland No. (0.5) turbidity

standard was applied into each of three wells of sterile 96-well flat-shaped bottom polystyrene microplates. The plates were incubated aerobically at 37°C for 24 hours. Afterwards, the microplates were rinsed thrice with deionized water, air-dried, and fixed by adding absolute methanol for 10 minutes. Thereafter, 200 µL of 0.1 % crystal violet was added to each well for 15 minutes. Once the staining reaction was done, repeated washing with deionized water was carried out. The plates were fully air-dried. Subsequently, 200 µL of 33 % glacial acetic acid was applied to each well for 10 min. The experiment was conducted in triplicates and as the negative control, the absorption of wells containing bacteria-free tryptic soy broth was used. By measuring the OD_{630} using a microplate reader (Biotek, UK), the amount of crystal violet obtained by the glacial acetic acid in each well was directly quantified [28].

To determine the effect of *A. australis* extract and NSH (at ½MIC) on biofilm of *E. coli*, the aforementioned protocol was applied.

2.7 Detection of fimH and mrkD

DNA was isolated from *E. coli*, using a G-spin™ extraction kit for bacteria (iNtRON, Korea) as directed by the manufacturer. The extracted DNA, primers (Table 1), and distributed maxime PCR premix™ (iNtRON, Korea) were thawed at 4°C, vortexed to ensure uniform contents and a 20 µL PCR mixture was made as stated by the manufacturer.

Table 1: Primers used in this study

Primer	Sequence 5′ - 3′	Amplicon size (bp)	Reference
fimH	F-ATTGCCGTGCTTATTTTGCGA	167	This study
	R-ATTGGCACTGAACCAGGGTAG		
mrkD	F-ATGTCGATGTGGGTTCCATCC	137	This study
	R-GAACGAGGTGCTAATGTTGGC		
*16S rRNA**	F-ACCTGGACTGATACTGACACTGA	-	[29]
	R-GTGGACTACCAGGGTATCTAATCCT		

*For RT PCR only

DNA was amplified using PCR reaction tubes in Master cycler gradient PCR (Eppendorff, Germany). Gradient PCR was used to optimize the temperature and time of the PCR. Following PCR, the amplicons were validated using 1.5% agarose gel electrophoresis.

2.8 Gene expression of fimH and mrkD

Trizol reagent (Promega, USA) was implemented to extract RNA from *E. coli* cells before and after the addition of NSH according to the protocol described by the manufacturer.

To evaluate the gene expression of *fimH* and *mrkD*. Moreover, after several trials, the thermo-cycler protocol was optimized. Expression levels were normalized to the housekeeping gene (*16S rRNA*). The difference in cycle thresholds (ΔCt) and fold changes were evaluated between the treated groups and the calibrators of each gene using Livak formula [30]:

$$\text{Fold change} = 2^{-\Delta\Delta Ct} \quad \text{.. (1)}$$

A fold change of less than 2-fold was considered insignificant [31]. A melting curve was obtained with temperatures ranging from 60°C to 95°C with a 1°C increase in temperature every one second

2.10 Statistical methods

Kolmogorov-Smirnov and Shapiro-Wilk tests were performed to test the normality distribution of data. Kruskal-Wallis H followed by Dunn's multiple comparisons test as a post hoc test was performed for comparing biofilm intensities. Two-way ANOVA followed by Tukey multiple comparison test for comparing the diameters of zones of inhibitions. The differences were considered significant when the P value ≤ 0.05. The statistical analysis was performed using GraphPad Prism 9.2 [32].

3. Results and Discussion

3.1. GC-MS study

Acalypha australis extract was assayed for the detection of bioactive compounds using GC-MS. The extract has shown the presence of various constituents involving 4-ethylbenzoic acid, cyclopentyl ester, 1,8-cineole, thymol, carvacrol, (+)-spathulenol, and bis-(2-ethylhexyl)-terephthalate (Figure 1 and Table 2).

Table 2: Detected molecules in the *Acalypha australis* extract using GC-MS.

No	RT (min)	Area (Abs)	Area %	Name	Quality
1	5.156	1176968	22.04	4-Ethylbenzoic acid, cyclopentyl ester	50
2	7.937	222812	4.17	1,8-Cineole	90
3	13.841	1059087	19.83	Thymol	95
4	14.044	760776	14.25	Carvacrol	91
5	20.005	247036	4.63	(+) spathulenol	38
6	37.413	1873633	35.08	Bis(2-ethylhexyl) terephthalate	35

RT: retention time; Abs: absorbance.

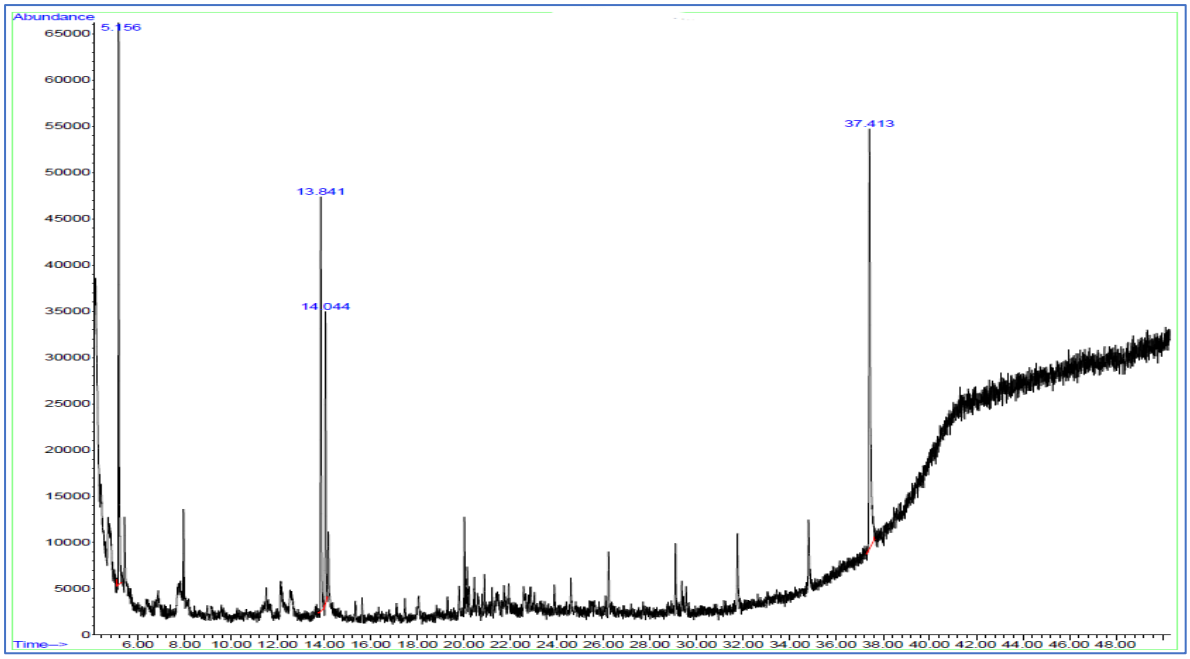

Figure 1: GC-MS spectrum of *Acalypha australis* aqueous extract.

Shafaie, et al. [33] reported the presence of many chemicals in *A. australis* leaves; nevertheless, none of which were match the present data. Locally, Al-Dobaissi [34] reported that *A. australis* extract contained varios bioactive compounds as benzuquinones, trihydroxyanthraquinones, brevifolin, gallic acid, rutin, kaempferol, loliolide, phytostroles, butanedioic acid, and niacin. Carvacrol was reported as a component of the methanol extract of *A. australis* in Selim, et al. [35] work. Carvacrol and thymol are phenolic compounds that are used for therapeutic actions with reducing properties [36] that can participate in the reduction of Ag^{+} to Ag^{0} creating silver nanoparticles (AgNPs). The highest intensity was observed for bis-(2-ethylhexyl)-terephthalate which was observed in the *A. australis* extract in the study of Badawy, et al. [37]. Thiemann [38] reported that phthalate compounds that are found in plant products, are from anthropogenic sources and in most cases are considered as contaminants. As for the rest of the constituents, no previous work has reported similar findings. The collective effect of chemicals in the plant extract can participate in the preparation of NSH and improve the antibacterial activity by overcoming bacterial resistance and introducing additives that increase the activity of the NSH against *E. coli*.

3.2 Characterization of A. australis Extract and nanocomposite of AgNPs and nanocomposite of silver and halloysite

3.2.1 XRD

Figure 2 depicts the characteristic XRD peaks of halloysite observed at 2θ including 11.804º, 20.658º, 26.811º, 29.526º, 36.122º, 39.559º, 47.911º, and 57.639º [39] with additional peaks which refers to nano-size Ag at 32.347º, 36.724º, 43.503º, and 64.901º with respective Miller incidences of 122, 111, 200, and 220 [40].

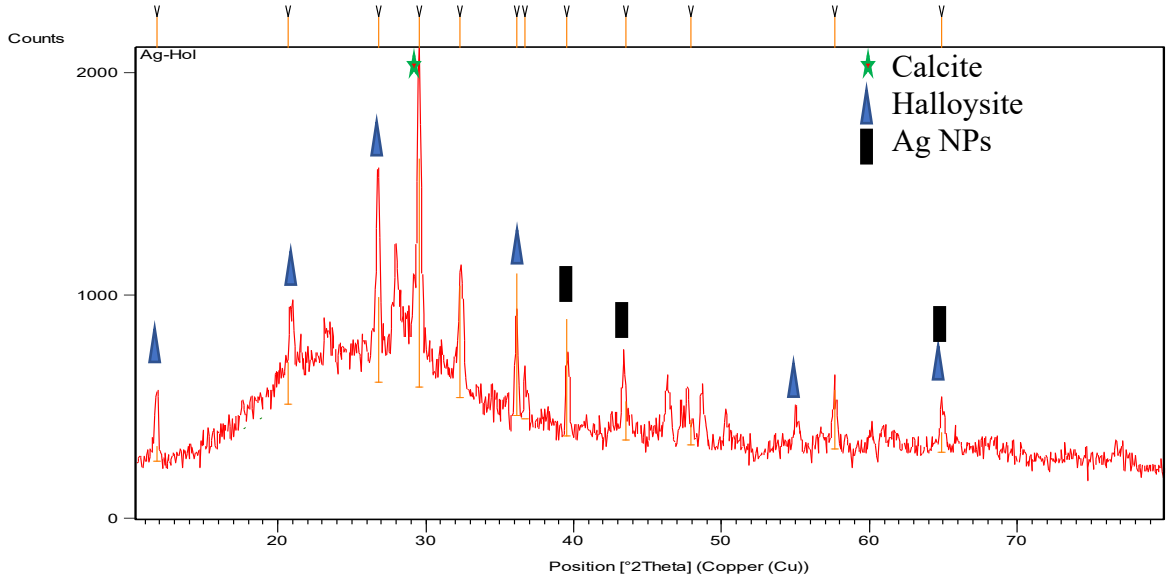

Figure 2: XRD of *AgNPs and* nanocomposite of silver and halloysite

The presence of these peaks could be solid evidence for the formation of the required nanocomposite (silver and halloysite). The measurement also exhibited a distinct peak at 29.5269° which was due to the calcite that was found as impurities within the halloysite. The particle size was calculated using the Scherrer equation for all peaks and the average particle size was found to be 35.97 nm, as illustrated in Table 3. Compared to the crystallite size calculated by the Scherrer equation for nanosilver and its composite with halloysite, the crystallite size increased from 25.32 nm in silver to 35.97 nm in the composite. The increase in crystallite size is additional evidence of structural changes that support the formation of the desired product.

Table 3: XRD data and average particle size of nanocomposite of silver and halloysite calculated using Scherer equation

Pos. [°2Th.]	Height [cts]	FWHM [°2Th.]	d-spacing [Å]	Particle size [nm]	Average particle size [nm]
11.8049	70.12	1.2358	7.49064	6.76	35.97
20.6582	189.70	2.5897	4.29609	3.26	

26.8114	386.31	1.4235	3.32248	6.00
29.5269	1024.69	0.5818	3.02281	14.76
32.3473	503.92	0.2834	2.76539	30.51
36.1228	641.00	0.0724	2.48455	120.64
38.9592	526.53	0.0690	2.27628	127.65
43.5033	176.55	0.8573	2.07861	10.43
47.9110	112.96	2.4350	1.89716	3.73
57.6393	268.53	0.1344	1.59795	70.52
64.9019	89.19	1.6357	1.43558	6.02

The current findings are in parallel with those obtained by Zou, et al. [41] and Guo, et al. [42] who loaded AgNPs on a halloysite nanotube using a green approach and revealed approximate peaks of XRD to the aforementioned 2θ.

3.2.2 TEM Study

The measurements revealed a distinctive structure of the prepared composite, as the measurements showed tube-like structures, which are the characteristic shape of halloysite tubes, which appeared as single or clustered tubes with a diameter not exceeding 13 nm. The measurements also showed dark particles with a diameter in the range of 10-17 nm and a shape that tends to be spherical, which represents the nanosilver, as it was compared with the nanosilver alone. The presence of both structures is evidence of the successful formation of the desired composite (Figure 3).

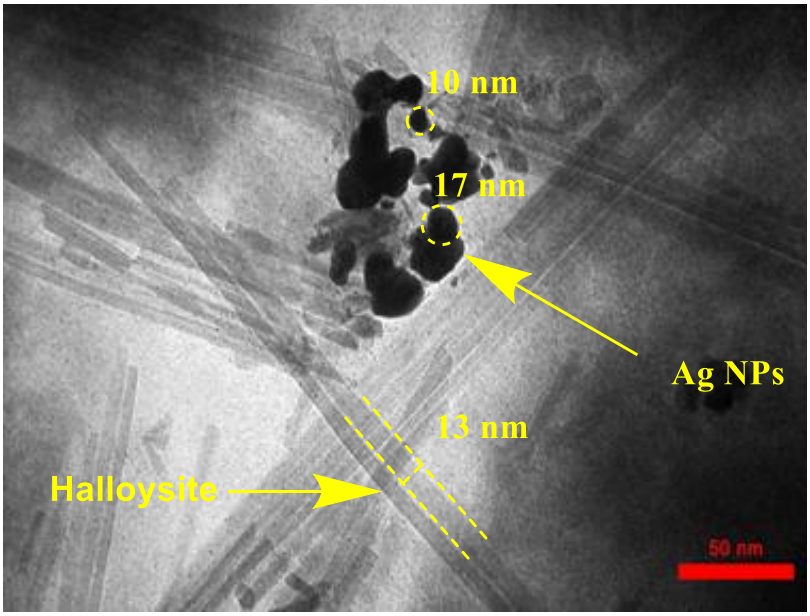

Figure 3: TEM of nanocomposite of silver and halloysite

Zou, et al. [41] indicated a cylinder shape of the NSH, but with heterogenous distribution of length. Moreover, the AgNPs were observed in the lumen of the halloysite as shown in the FESEM image, where similar data was previously reported by Guo, et al. [42].

3.3 Inhibitory effect of Acalypha australis extract and nanocomposite of silver and halloysite

The outcomes in Figure 4 suggest that *A. australis* extract exhibited a constantly smaller area of inhibition in comparison to NSH, throughout all concentrations. Insignificant differences were observed among the tested concentrations of *A. australis* extract, highlighting the raising of extract concentrations does not necessarily increase the inhibitory action. Concerning the inhibitory action of NSH increased with respect to the increase of concentration. Given that, in comparison to the zone of inhibition at 25% concentration is smaller than 50 and 100% ($P< 0.05$). Nonetheless, 50 and 100% inhibitory activity showed insignificant differences ($P> 0.05$) revealing that concentrations more than 50% may not bring about a significantly large inhibitory impact. NSH at 50% and 100% concentrations revealed considerably ($P< 0.0001$) larger inhibition zones in comparison to all concentrations of *A. australis* extract, demonstrating a highly potent antimicrobial activity. The most important difference ($P < 0.0001$) is quite visible between NSH at 100% and *A. australis* extract at 25%, indicating that NSH is much more powerful than the extract at lower or similar concentrations.

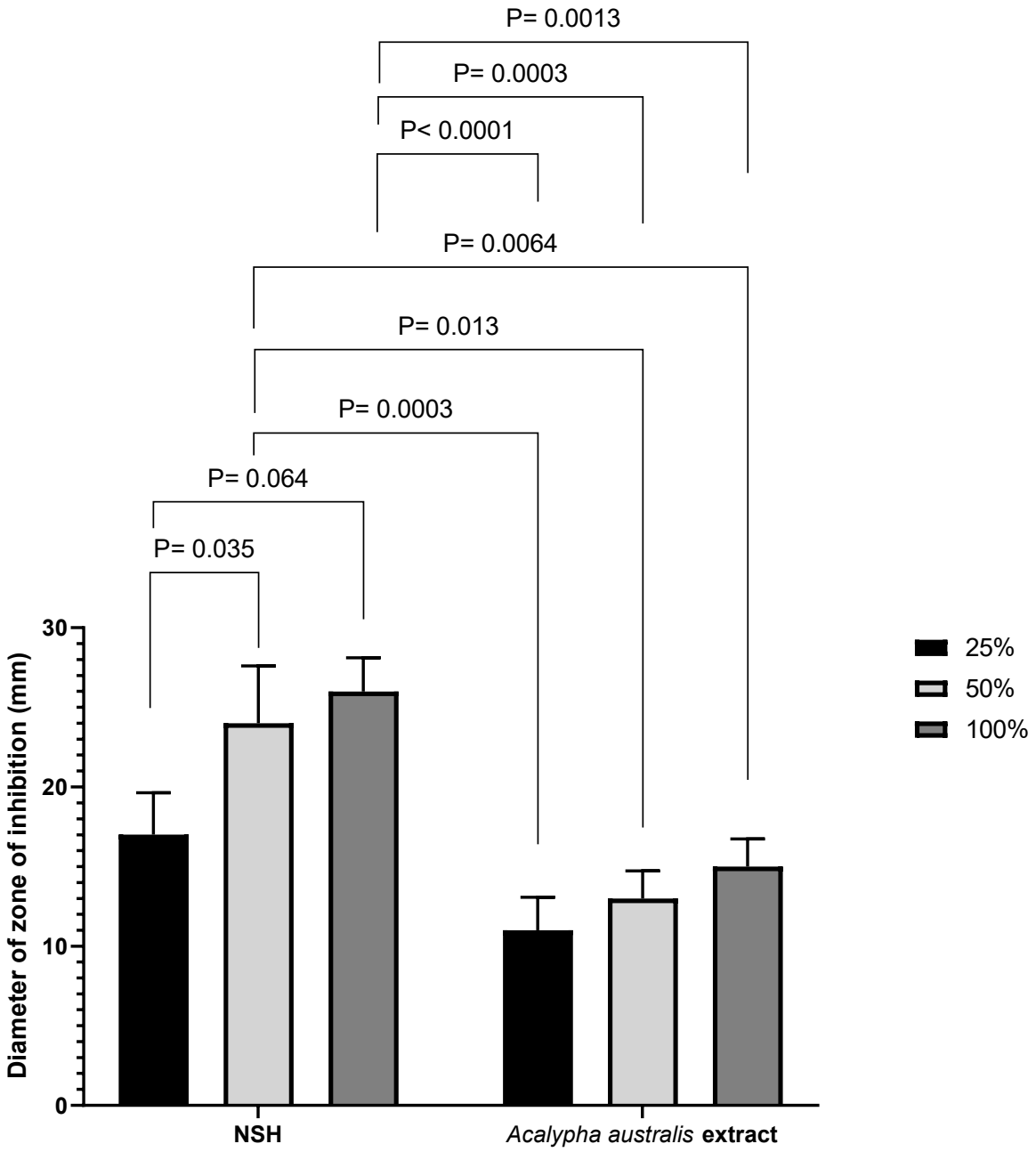

Figure 4: The inhibition zone of *E. coli* caused by *A. australis* extract and nanocomposite of silver and halloysite (NSH).

3.4 Effect of nanocomposite of silver and halloysite *and Acalypha australis extract on Biofilm*

A significant reduction (P<0.0001) in biofilm intensity was observed upon the use of *A. australis* extract and NSH highlighting that both compounds have potent antibiofilm efficacy (Figure 5). However, the mode of action might differ, concerning *A. australis* extract could exhibit antimicrobial activity owing to its content of phytochemical compounds (Table 2)

including phenolics (Carvacrol and thymol) [43], 1,8-Cineole [44], and (+) spathulenol [45], whereas the NSH potentially eliminate biofilm through antimicrobial characteristics of silver as well as the halloysite capability to deliver nanoparticles efficiently [46]. Similarly, Cherednichenko, et al. [47] documented that NSH markedly inhibit biofilm formation in *Serratia marcescens***.** Nonetheless, insignificant differences (P>0.05) were noticed between the *A. australis* extract and NSH as illustrated in Figure 4, indicating that both treatments were equivalently effective in decreasing biofilm intensity.

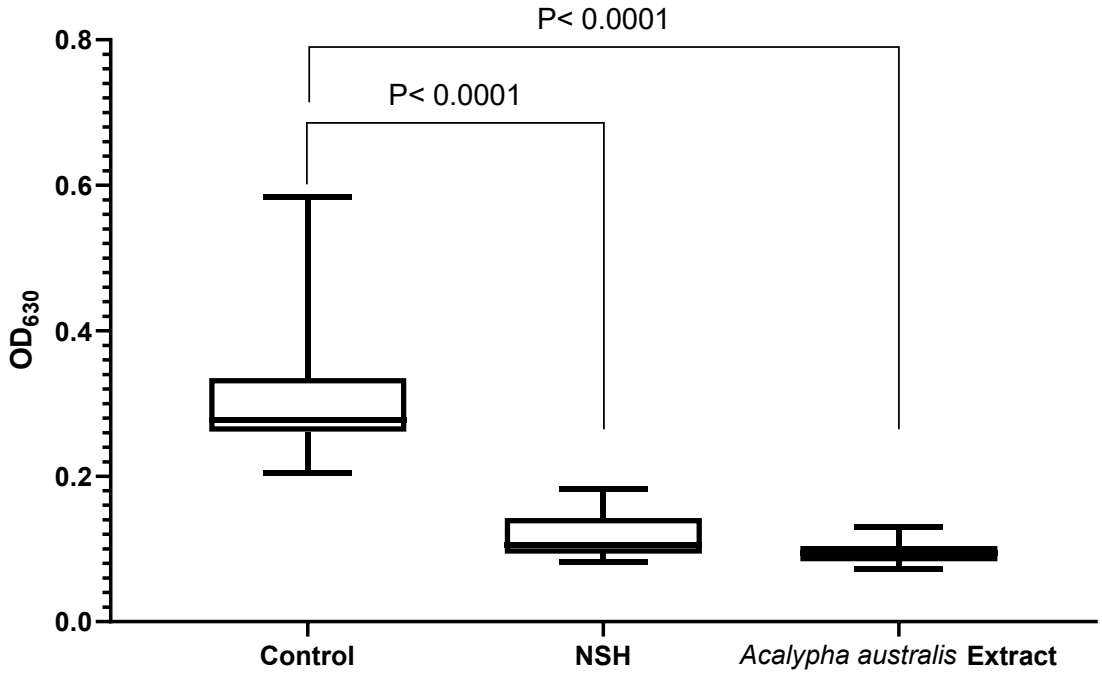

Figure 5: Effect of *Acalypha australis* extract and nanocomposite of silver and halloysite (NSH) on the biofilm intensity of *E. coli*

The growth inhibition results agreed with the biofilm data, where both *A. australis* extract and NSH exhibited anti-*E. coli* properties, as shown in Figure 5.

3.5 Detection of fimH and mrkD

The *mrkD* gene was detected in 23 (88.4%) *E. coli* isolates (Figure 6A); however, *fimH* gene was detected in all *E. coli* isolates (Figure 6B). This was consistence with Hasan, et al. [48] as they located the *fimH* gene in all *E. coli* strains isolated from patients with cystitis. Ghafer, et al. [49] found that 95.6% of uropathogenic *E. coli* harboured *fimH*. On the other

hand, Alzrkani and Abdulkareem [50] stated that only 2 out of 5 *E. coli* isolates carried *fimH*. Khonsari, et al. [14] indicated that Only 2% of uropathogenic *E. coli* isolated from patients with non-catheter-associated UTIs carried *mrkD*.

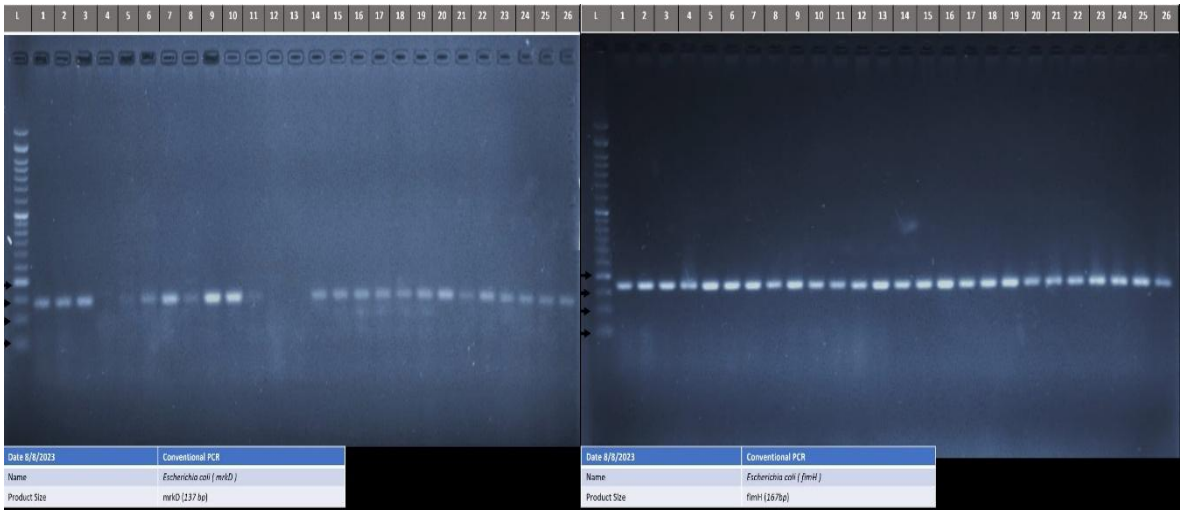

(A) **(B)**

Figure 6: Agarose gel electrophoresis for *mrkD* (A) and *fimH* (B) genes in *E. coli*.

3.6 Gene expression of *mrkD* and *fimH*

The findings grouped in Figure 7 revealed that both genes were downregulated by the action of NSH, where the fold change of *mrkD* and *fimH* reached 0.297 ± 0.140 and 0.325 ± 0.202, respectively. Such results indicate that the inhibition of biofilm (Figure 7) is mediated by *mrkD* and *fimH* downregulation, which previously mentioned that both genes play an essential role in biofilm formation [11, 14]. Ong, et al. [51] reported that *mrkD* deletion mutant *E. coli* developed significantly lower biofilm intensity than their respective wild type.

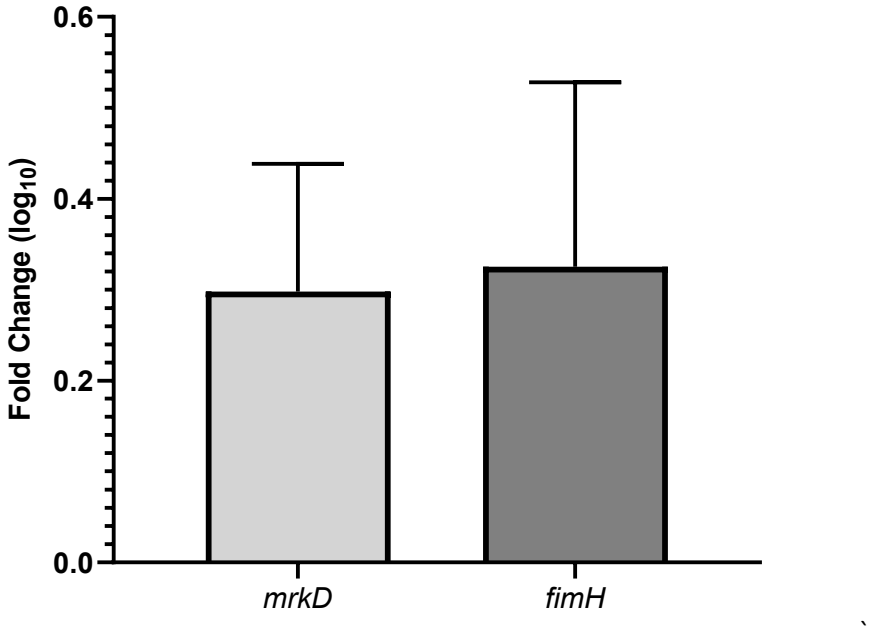

Figure 7: Fold change of *mrkD* and *fimH* in *E. coli*. Error bars denote standard deviation.

Conclusion

The study proved that using ultrasound assisted method, the nanocomposite of silver with halloysite was formed rapidly with high stability of the composite, which resulted from the presence of halloysite as an additional stabilizer in addition to the extract, whose components proved their ability to reduce and bind silver without structural change in the clay composition, as proven by X-ray diffraction. Using the method designed to prepare these composite, silver was formed with sizes not exceeding 17 nm decorated to halloysite tubes with a diameter not exceeding 13 nm, as proven by transmission electron microscopy.

At comparable concentrations, the antimicrobial and antibiofilm efficacy of NSH is more powerful than the *A. australis* extract. Given that both *mrkD* and *fimH* were downregulated by the action of NSH. Such results implied that the antibiofilm activity is mediated by the downregulation of *mrkD* and *fimH*.

Acknowledgements

None

Conflict of Interest

None

Funding

None

Contribution

The authors have a same contribution.

Ethical Approval:

The study was conducted following the receipt of participant consent and ethical approval from the Ethics Committee of the Biology Department at the University of Baghdad, College of Science no. (Ref.CSEC/0526/0049) on May. This procedure is in line with the guidelines set forth by the Iraqi Ministry of Health and Environment**.**

References

[1] M. Frieri, K. Kumar, and A. Boutin, "Antibiotic resistance," *Journal of Infection and Public Health,* vol. 10, no. 4, pp. 369-378, 2017/07/01/ 2017, doi: https://doi.org/10.1016/j.jiph.2016.08.007.

[2] D. G. J. Larsson and C.-F. Flach, "Antibiotic resistance in the environment," *Nature Reviews Microbiology,* vol. 20, no. 5, pp. 257-269, 2022/05/01 2022, doi: https://doi.org/10.1038/s41579-021-00649-x.

[3] C. M. Ardila, J. A. Bedoya-García, and D. E. Arrubla-Escobar, "Antibiotic resistance in periodontitis patients: A systematic scoping review of randomized clinical trials," *Oral diseases,* vol. 29, no. 7, pp. 2501-2511, 2023.

[4] J. Bengtsson-Palme, E. Kristiansson, and D. G. J. Larsson, "Environmental factors influencing the development and spread of antibiotic resistance," *FEMS Microbiology Reviews,* vol. 42, no. 1, 2017, doi: 10.1093/femsre/fux053.

[5] E. Larson, "Community factors in the development of antibiotic resistance," *Annu. Rev. Public Health,* vol. 28, pp. 435-447, 2007.

[6] E. M. Darby, E. Trampari, P. Siasat, M. S. Gaya, I. Alav, M. A. Webber, and J. M. A. Blair, "Molecular mechanisms of antibiotic resistance revisited," *Nature Reviews Microbiology,* vol. 21, no. 5, pp. 280-295, 2023/05/01 2023, doi: 10.1038/s41579-022-00820-y.

[7] N. Høiby, T. Bjarnsholt, M. Givskov, S. Molin, and O. Ciofu, "Antibiotic resistance of bacterial biofilms," *International Journal of Antimicrobial Agents,* vol. 35, no. 4, pp. 322-332, 2010/04/01/ 2010, doi: https://doi.org/10.1016/j.ijantimicag.2009.12.011.

[8] T. Tolker-Nielsen, "Biofilm Development," in *Microbial Biofilms*, 2015, pp. 51-66.

[9] E. Denamur, O. Clermont, S. Bonacorsi, and D. Gordon, "The population genetics of pathogenic Escherichia coli," *Nature Reviews Microbiology,* vol. 19, no. 1, pp. 37-54, 2021/01/01 2021, doi: 10.1038/s41579-020-0416-x.

[10] N. N. Yaseen and H. J. Al-Mathkhury, "Effectiveness of some β-lactamase encoding genes on biofilm formation and slime layer production by uropathogenic Escherichia coli," *World Journal of Experimental Biosciences (ISSN: 2313-3937),* pp. 61-68, 2015.

[11] N. Foroogh, M. Rezvan, K. Ahmad, and S. Mahmood, "Structural and functional characterization of the FimH adhesin of uropathogenic Escherichia coli and its novel applications," *Microbial Pathogenesis,* vol. 161, p. 105288, 2021/12/01/ 2021, doi: https://doi.org/10.1016/j.micpath.2021.105288.

[12] M. A. Schembri, K. Kjaergaard, E. V. Sokurenko, and P. Klemm, "Molecular Characterization of the Escherichia coli FimH Adhesin," *The Journal of Infectious Diseases,* vol. 183, no. Supplement_1, pp. S28-S31, 2001, doi: 10.1086/318847.

[13] L. Mousavifar, M. Sarshar, C. Bridot, D. Scribano, C. Ambrosi, A. T. Palamara, G. Vergoten, B. Roubinet, L. Landemarre, J. Bouckaert, and R. Roy, "Insightful Improvement in the Design of Potent Uropathogenic E. coli FimH Antagonists," *Pharmaceutics,* vol. 15, no. 2, p. 527, 2023. [Online]. Available: https://www.mdpi.com/1999-4923/15/2/527.

[14] M. S. Khonsari, P. Behzadi, and F. Foroohi, "The prevalence of type 3 fimbriae in Uropathogenic Escherichia coli isolated from clinical urine samples," *Meta Gene,* vol. 28, p. 100881, 2021/06/01/ 2021, doi: https://doi.org/10.1016/j.mgene.2021.100881.

[15] Fahim, M., Shahzaib, A., Nishat, N., Jahan, A., Bhat, T. A., & Inam, A. (2024). Green Synthesis of Silver Nanoparticles: A Comprehensive Review of Methods, Influencing Factors, and Applications. *JCIS Open*, 100125.

[16] Arshad, F., Naikoo, G. A., Hassan, I. U., Chava, S. R., El-Tanani, M., Aljabali, A. A., & Tambuwala, M. M. (2024). Bioinspired and green synthesis of silver nanoparticles for medical applications: a green perspective. *Applied Biochemistry and Biotechnology*, *196*(6), 3636-3669.

[17] Nguyen, N. P. U., Dang, N. T., Doan, L., & Nguyen, T. T. H. (2023). Synthesis of silver nanoparticles: from conventional to 'modern'methods—a review. *Processes*, *11*(9), 2617.

[18] Shihab, I. A., Muhammed, M. Y., Alheety, M. A., & Alheety, N. F. (2023). Ultrasound assisted rapid synthesis of Pd/PdO binary nanorod alloy as hydrogen storage enhancer for GO-Pd/PdO nanocomposite. *Chemical Data Collections*, *47*, 101074.

[19] Shekhar, S., Prakash, P., Shekhar, S., Singh, S. K., & Prasad, K. (2023, December). Ultrasound-assisted green synthesis of silver nanoparticles from Allium sativum, its characterization, antimicrobial capabilities and thermo-plasmonic studies. In *Journal of Physics: Conference Series* (Vol. 2663, No. 1, p. 012020). IOP Publishing.

[20] Abdulkareem, S. M., Alsaffar, R. M., Razzaq, G. H. A., Mohammed, J. H., Awad, T. M., Alheety, M. A., ... & Ghotekar, S. (2024). Effect of direct and indirect in-situ sonochemical synthesis methods of MWCNTs–CoNiFerrite on the hydrogen storage. *Journal of Sol-Gel Science and Technology*, *111*(3), 979-988.

[21] Allawi, A. H., Mohammed, M. Y., Ayrim, N. B., Alheety, M. A., & Mahmood, A. R. (2022). Synthesis of attapulgite-MnO2 nanocomposite from manganese complex by ultrasound for hydrogen storage. *Journal of the Indian Chemical Society*, *99*(8), 100596.

[22] Abdulkareem, M. A., Joudi, M. S., & Ali, A. H. (2022). Eco-friendly synthesis of low-cost antibacterial agent (brown attapulgite-Ag nanocomposite) for environmental application. *Chemical Data Collections*, *37*, 100814.

[23] Jiang, Z., Sun, S., Liu, J., & Sun, X. (2024). Recent advances of halloysite nanotubes in biomedical applications. *Small*, *20*(2), 2306169.

[24] Boraei, S. B. A., Eshghabadi, F., Hosseinpour, R., Zare, Y., Munir, M. T., & Rhee, K. Y. (2024). Halloysite nanotubes in biomedical applications: Recent approaches and future trends. *Applied Clay Science*, *253*, 107346.

[25] N. A. Baeshen, Y. Q. Almulaiky, M. Afifi, A. Al-Farga, H. A. Ali, N. N. Baeshen, M. M. Abomughaid, A. M. Abdelazim, and M. N. Baeshen, "GC-MS Analysis of Bioactive Compounds Extracted from Plant Rhazya stricta Using Various Solvents," (in eng), *Plants (Basel),* vol. 12, no. 4, Feb 20 2023, doi: 10.3390/plants12040960.

[26] X. Zhang and M. Heidari Majd, "Synthesis of halloysite nanotubes decorated with green silver nanoparticles to investigate cytotoxicity, lipid peroxidation and induction of apoptosis in acute leukemia cells," *Scientific Reports,* vol. 13, no. 1, p. 17182, 2023/10/11 2023, doi: 10.1038/s41598-023-43978-y.

[27] F. Mytlak, M. Jabir, U. Naif, and H. Fadhil, "Synthesis and characterization of Au nanoparticles for nanomedicine application," *Iraqi Journal of Physics,* vol. 15, pp. 109-116, 2017.

[28] A. Bras, M. Braz, I. Martinho, J. Duarte, C. Pereira, and A. Almeida, "Effect of Bacteriophages against Biofilms of Escherichia coli on Food Processing Surfaces," *Microorganisms,* vol. 12, no. 2, Feb 10 2024, doi: 10.3390/microorganisms12020366.

[29] M. J. H. Goldsworthy, "Gene expression of Pseudomonas aeruginosa and MRSA within a catheter-associated urinary tract infection biofilm model," *Bioscience Horizons,* vol. 1, no. 1, pp. 28-37, 2008.

[30] K. J. Livak and T. D. Schmittgen, "Analysis of relative gene expression data using real-time quantitative PCR and the 2(-Delta Delta C(T)) Method," (in eng), *Methods,* vol. 25, no. 4, pp. 402-8, Dec 2001, doi: 10.1006/meth.2001.1262.

[31] J. P. Rasigade, A. Moulay, Y. Lhoste, A. Tristan, M. Bes, F. Vandenesch, J. Etienne, G. Lina, F. Laurent, and O. Dumitrescu, "Impact of sub-inhibitory antibiotics on fibronectin-mediated host cell adhesion and invasion by Staphylococcus aureus," *BMC Microbiol,* vol. 11, p. 263, Dec 14 2011, doi: 10.1186/1471-2180-11-263.

[32] M. Pagano, K. Gauvreau, and H. Mattie, *Principles of biostatistics*, 3rd ed. New York: Chapman and Hall/CRC., 2022.
[33] F. Shafaie, S. Aramideh, O. Valizadegan, M. H. Safaralizadeh, and N. N. Pesyan, "GC/MS analysis of the essential oils of Cupressus arizonica Greene, Juniperus communis L. and Mentha longifolia L," *Bulletin of the Chemical Society of Ethiopia,* vol. 33, no. 3, pp. 389-400, 2019, doi: https://dx.doi.org/10.4314/bcse.v33i3.1.
[34] I. Al-Dobaissi, "Chemical analysis of new record species Acalypha australis L. at Iraq," *Iraqi Journal of Agricultural Sciences,* vol. 54, no. 3, pp. 674-681, 2023.
[35] S. A. Selim, M. E. Adam, S. M. Hassan, and A. R. Albalawi, "Chemical composition, antimicrobial and antibiofilm activity of the essential oil and methanol extract of the Mediterranean cypress (Cupressus sempervirens L.)," *BMC Complementary and Alternative Medicine,* vol. 14, no. 1, p. 179, 2014/06/02 2014, doi: 10.1186/1472-6882-14-179.
[36] H. H. Agus, "Chapter 4 - Terpene toxicity and oxidative stress," in *Toxicology*, V. B. Patel and V. R. Preedy Eds.: Academic Press, 2021, pp. 33-42.
[37] M. E. Badawy, I. E. Kherallah, A. S. Mohareb, M. Salem, and H. A. Yousef, "Chemical composition and antimicrobial activity of bark and leaf extracts of Cupressus sempervirens and Juniperus phoenicea grown in Al-Jabel Al-Akhdar Region, Libya," *The Natural Products Journal,* vol. 9, no. 4, pp. 268-279, 2019, doi: https://doi.org/10.2174/2210315508666180223151210.
[38] T. Thiemann, "Isolation of phthalates and terephthalates from plant material–natural products or contaminants?," *Open Chemistry Journal,* vol. 8, no. 1, 2021, doi: http://dx.doi.org/10.2174/1874842202108010001.
[39] N. Tamsu Selli, I. M. Aker, N. Basaran, and E. Kabakci, "Influence of calcined halloysite on technological & mechanical properties of wall tile body," *Journal of Asian Ceramic Societies,* vol. 9, no. 3, pp. 1331-1344, 2021/07/03 2021, doi: https://doi.org/10.1080/21870764.2021.1974762.
[40] Y. Meng, "A Sustainable Approach to Fabricating Ag Nanoparticles/PVA Hybrid Nanofiber and Its Catalytic Activity," *Nanomaterials,* vol. 5, no. 2, pp. 1124-1135, 2015. [Online]. Available: https://www.mdpi.com/2079-4991/5/2/1124.
[41] M. Zou, M. Du, H. Zhu, C. Xu, and Y. Fu, "Green synthesis of halloysite nanotubes supported Ag nanoparticles for photocatalytic decomposition of methylene blue," *Journal of Physics D: Applied Physics,* vol. 45, no. 32, p. 325302, 2012/07/30 2012, doi: https://doi.org/10.1088/0022-3727/45/32/325302.
[42] W. Guo, W. Liu, L. Xu, P. Feng, Y. Zhang, W. Yang, and C. Shuai, "Halloysite nanotubes loaded with nano silver for the sustained-release of antibacterial polymer nanocomposite scaffolds," *Journal of Materials Science & Technology,* vol. 46, pp. 237-247, 2020/06/01/ 2020, doi: https://doi.org/10.1016/j.jmst.2019.11.019.
[43] S. Peter, N. Sotondoshe, and B. A. Aderibigbe, "Carvacrol and Thymol Hybrids: Potential Anticancer and Antibacterial Therapeutics," (in eng), *Molecules,* vol. 29, no. 10, May 12 2024, doi: 10.3390/molecules29102277.
[44] R. Pries, S. Jeschke, A. Leichtle, and K. L. Bruchhage, "Modes of Action of 1,8-Cineol in Infections and Inflammation," (in eng), *Metabolites,* vol. 13, no. 6, Jun 13 2023, doi: 10.3390/metabo13060751.
[45] H. Ammar, Y. M'Rabet, S. Hassan, M. Chahine, M. de Haro-Marti, W. Soufan, S. Andres, S. López, and K. Hosni, "Chemodiversity and antimicrobial activities of Eucalyptus spp. essential oils," *Cogent Food & Agriculture,* vol. 10, no. 1, p. 2383318, 2024/12/31 2024, doi: 10.1080/23311932.2024.2383318.
[46] S. Rakshit, T. Roy, P. C. Jana, and K. Gupta, "A Comprehensive Review on the Importance of Sustainable Synthesized Coinage Metal Nanomaterials and Their Diverse Biomedical Applications," *Biol Trace Elem Res,* Sep 2 2024, doi: 10.1007/s12011-024-04361-8.
[47] Y. Cherednichenko, S. Batasheva, F. Akhatova, R. Fakhrullin, and E. Rozhina, "Antibiofilm activity of silver nanoparticles-halloysite nanocomposite in Serratia marcescens," *Journal of Nanoparticle Research,* vol. 26, no. 4, p. 71, 2024/04/02 2024, doi: 10.1007/s11051-024-05971-y.

[48] R. N. Hasan, S. A. Jasim, and Y. H. Ali, "Detection of fimH, kpsMTII, hlyA, and traT genes in Escherichia coli isolated from Iraqi patients with cystitis," *Gene Reports,* vol. 26, p. 101468, 2022/03/01/ 2022, doi: https://doi.org/10.1016/j.genrep.2021.101468.

[49] A. Ghafer, A. Ghareeb, and S. Mohaisen, "The Prevalence of FimH and TosA Genes in Escherichia coli Isolated from Urinary Tract Infections," *Iraqi Journal of Biotechnology,* vol. 21, no. 1, pp. 79-88, 2022.

[50] M. Alzrkani and R. Abdulkareem, "Uropathogenic Escherichia coli Antibiotic Resistance and in silico Virtual Screening Using Pharmit Technique," *Iraqi Journal of Biotechnology,* vol. 21, pp. 26-41, 2022.

[51] C. L. Ong, S. A. Beatson, M. Totsika, C. Forestier, A. G. McEwan, and M. A. Schembri, "Molecular analysis of type 3 fimbrial genes from Escherichia coli, Klebsiella and Citrobacter species," (in eng), *BMC Microbiol,* vol. 10, p. 183, Jun 24 2010, doi: 10.1186/1471-2180-10-183.